Nanoscale

PAPER

View Article Online
View Journal | View Issue

Cite this: *Nanoscale*, 2024, **16**, 15358

Accelerating and breaking adaptive nano-colloids (<100 nm) into unsteady state operation *via* push–pull effects†

Cornelia Lanz, Nele Künnecke, Yaşar Krysiak and Sebastian Polarz *

Received 15th April 2024,
Accepted 26th July 2024

DOI: 10.1039/d4nr01644k

rsc.li/nanoscale

Unlike conventional colloids showing random mobility because of Brownian motion, active colloids contain nanomotors that translate chemical or physical triggers into directed movement. Whereas the acceleration of such particles works well, it is difficult to decelerate them by request. Compared to the existing literature on microscaled swimmers/robots, the main question of the current paper is whether nanoscaled colloids (<100 nm) can also be actively controlled despite the stronger relevance of rotational diffusion at such dimensions. We developed nanoparticles comprising two independent mechanisms for propulsion: a chemical engine associated with a Janus-type modification of organosilica nanoparticles and physical locomotion because of a superparamagnetic core inside these particles. Both triggers can be used independently to initiate the particles' directed and anisotropic movement. The magnetic forces can be tuned, most importantly concerning the angle defining the chemical acceleration. Superposition and a boost state are adopted for a parallel alignment. However, when the magnetic field acting on the particles is turned to an antiparallel orientation, a rapid deceleration can be observed, and the colloids halt.

Introduction

One of the highest goals in material science is the generation of so-called active matter,[1] similar to how it is currently found only in biological systems.[2] A prerequisite is that the constituents can dissipate energy catalyzed into collective behavior and properties.[3] In this context, fascinating discoveries have been made with the help of unique colloidal particles. So-called active colloids are smart systems that react to external and environmental conditions.[4–6] For instance, they are used to understand swarming behavior[7,8] or open new perspectives in active matter therapeutics.[9] Complex and directed transport processes can be realized by developing motorized nanoparticles with an efficient energy conversion to overcome the random Brownian motion.[10–12]

A first generation of such particles containing autonomous nanomotors uses chemicals in the environment as fuels and their decomposition for different propulsion mechanisms.[13,14] The most typical examples are enzyme-powered nanomotors that convert glucose or urea.[15,16] However, there is no control over the direction of movement unless one implements an anisotropic functionalization of the colloid surfaces. The nanoparticle architecture becomes crucial, and the so-called Janus-type architecture can be observed as a dominant feature in the literature.[17,18] The asymmetry is the basis for directed propulsion. The mobility of the particles depends on many factors, most importantly, their size and mass.

A shortcoming of chemical-driven nanomotors is the lack of *in situ* regulation of the speed, deceleration, and difficulties in motion direction. The success of the concept to equip colloids with different kind of motors has been presented in the literature by the pioneering work by multiple research groups such as Baraban *et al.*,[19,20] Das *et al.*[21] or Schattling *et al.*[22] The group of Pumera *et al.* has discussed in several articles unique perspectives for applying robotic colloids, for instance, in *in vivo* applications, water purification, or learning about swarming behavior.[23–25] The combination of two engines in one nanoparticle is valuable and, in turn, implies even more complex requirements for the colloid design.[26] Physical triggers like an external field combined with chemical propulsion

Institute of Inorganic Chemistry, Leibniz Universität Hannover, Callinstrasse 9, D-30167 Hannover, Germany. E-mail: sebastian.polarz@aca.uni-hannover.de

† Electronic supplementary information (ESI) available: Supplementary experimental section, methods and data. (PDF). Video S1. Motion video of dual nanomotors without propulsion. (MP4). Video S2 and S3. Motion videos of dual nanomotors under magnetic propulsion with different orientation of external magnetic field. (MP4). Video S4. Motion video of dual nanomotors under chemical propulsion with 50 mM glucose as fuel. (MP4). Video S5. Motion video of dual nanomotors under chemical propulsion with glucose used in a gradient. (MP4). Video S6. Motion video of dual nanomotors under dual propulsion in boost mode with same orientation of magnet and increasing glucose concentration. (MP4). Video S7. Motion video of dual nanomotors under dual propulsion in brake mode with opposite orientation of magnet and increasing glucose concentration. (MP4). See DOI: https://doi.org/10.1039/d4nr01644k

can greatly enhance the system's adjustability. Examples of active colloids in the literature address a chemical engine combined with a physical such as an external field or light.[27–29] Shao *et al.* reported a seesaw effect using a twin-engine nanomotor based on bowl-shaped polymer nanoparticles and Au-capping with H_2O_2 and near-infrared (NIR) propulsion working together.[28] Despite the interesting results of combining chemical and light-triggered propulsion in an active colloid, a physical stimulus characterized by a more stringent directionality is highly relevant to the current paper. A magnetic field in combination with chemical-triggered propulsion fulfils the latter requirement.[30–33] Thereby, push–pull effects, namely the chemical propulsion by consuming a fuel and the magnetic propulsion induced by a magnetic field could be utilized with great flexibility. Depending on direction of the magnetic field in relation to the fuel-induced movement, such push–pull effects could complement each other and boost the movement or even be competitive for an opposing setup. The vast majority of the materials presented in the past literature is on particles with sizes above 1μm. Because of the micron dimension of the colloids dissipation of energy by friction is a dominant factor and makes the systems highly damped.

Therefore, the idea is straightforward to use nano-sized Janus particles and perform analogical investigations. Not only is preparing Janus particles with sizes well below 100 nm highly difficult, but another fundamental question scrutinizes the latter concept. The smaller the particles become, the more they are susceptible to randomization of movement and orientations by thermal fluctuations. Because of the given arguments, we believe that it is highly interesting to investigate nano-scaled colloids possessing two independent types of accelerations, as shown in Scheme 1.

We have recently presented nanoparticle amphiphiles based on organosilica chemistry.[34,35] Each particle consists of a magnetic core, and compared to other active colloids, small size and low mass make the nanoparticles prone to fast acceleration. However, we have not integrated chemical propulsion in those past cases. The concept of the current paper is demonstrated in Scheme 1. The Janus architecture of the organosilica shell is designed to grant effective chemical propulsion. Then, the direction of the vector describing the acceleration (a_{chem}) due to chemical propulsion is parallel to the dipole defined by the Janus modification. It cannot change direction. As acceleration is a vectorial property, the force by an external magnetic field will also add to it (a_{mag}). We found in our recent paper[35] that for spherical particles, the domain of the superparamagnetic core can be oriented freely inside a magnetic field without exerting a torque on the particle as a whole. Therefore, as shown in Scheme 1, we expect one to vary the angle θ between a_{chem} and a_{mag}. This will directly affect the value and direction of the effective diffusion coefficient D_{eff}. With this system, the acceleration and deceleration of 50 nm-sized motors can be influenced *via* a controlled use of the chemical and physical engine in a complementary and contrary way. In particular, applying a break for the particle movement has seldom been at the center of scientific investigations in the mentioned previous literature on micro-scaled particles.

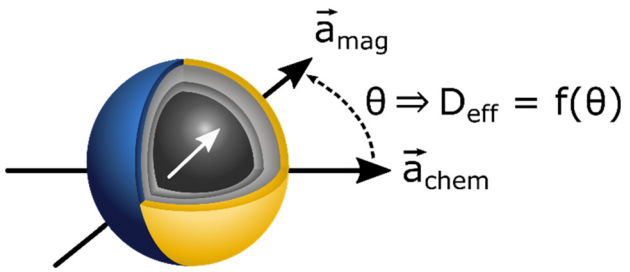

Scheme 1 Planned architecture of adaptive colloids: Janus-type (blue/yellow) organosilica nanoparticles contain a superparamagnetic core (black) whose magnetic domain (white arrow) can be oriented in a magnetic field and accelerate the particle (a_{mag}). The external magnetic field strength and direction determine the particles' acceleration due to the magnetic force. The chemical engine's reaction rate influences the acceleration due to propulsion (a_{chem}). Because one can adjust the angle between those two factors, the mobility of the particles expressed by the effective diffusion coefficient D_{eff} will be affected.

Results and discussion

The paper's first section describes the synthesis of novel superparamagnetic Janus-type nanoparticles comprising a chemical engine powered by biofuel. We will then characterize the mobility of the colloids impelled by the two triggers separately from each other. Finally, the mobility will be investigated if both factors are active, chemical propulsion and magnetic force, and are aligned in different directions.

Synthesis and characterization of Janus nanomotors

The starting organosilica core–shell (CS) nanoparticles consisting of a spherical magnetite core and an organosilica shell were prepared in analogy to our preliminary work;[34] see also the experimental part described in the ESI.† Briefly, the magnetite cores are covered by a pure silica shell using an inverse microemulsion method,[36] followed by the condensation of an alkyne-containing organosilica precursor as the second shell. The alkyne groups can easily be functionalized *via* photo-induced thiol–yne click chemistry.[37] The characterization of CS nanoparticles with a diameter of 46.5 nm (polydispersity index (PDI) = 5.4%), including transmission electron microscopy (TEM), infrared (IR) spectroscopy, dynamic light scattering (DLS), superconducting quantum interference device (SQUID) measurements and powder X-ray diffraction (PXRD) were summarized in ESI Fig. S1.†

Fig. 1 shows the Janus-type attachment of the functional groups needed for chemical propulsion to the surfaces of the CS particles. On one particle hemisphere, H_2O_2 is produced enzymatically from glucose using glucose oxidase (GOx). H_2O_2 is then further decomposed to O_2(g) by Pt on the second hemisphere for bubble propulsion. For realizing the Janus architecture, the CS particles are densely packed in a monolayer on a silicon/zinc oxide (ZnO) wafer, followed by sputter coating of a

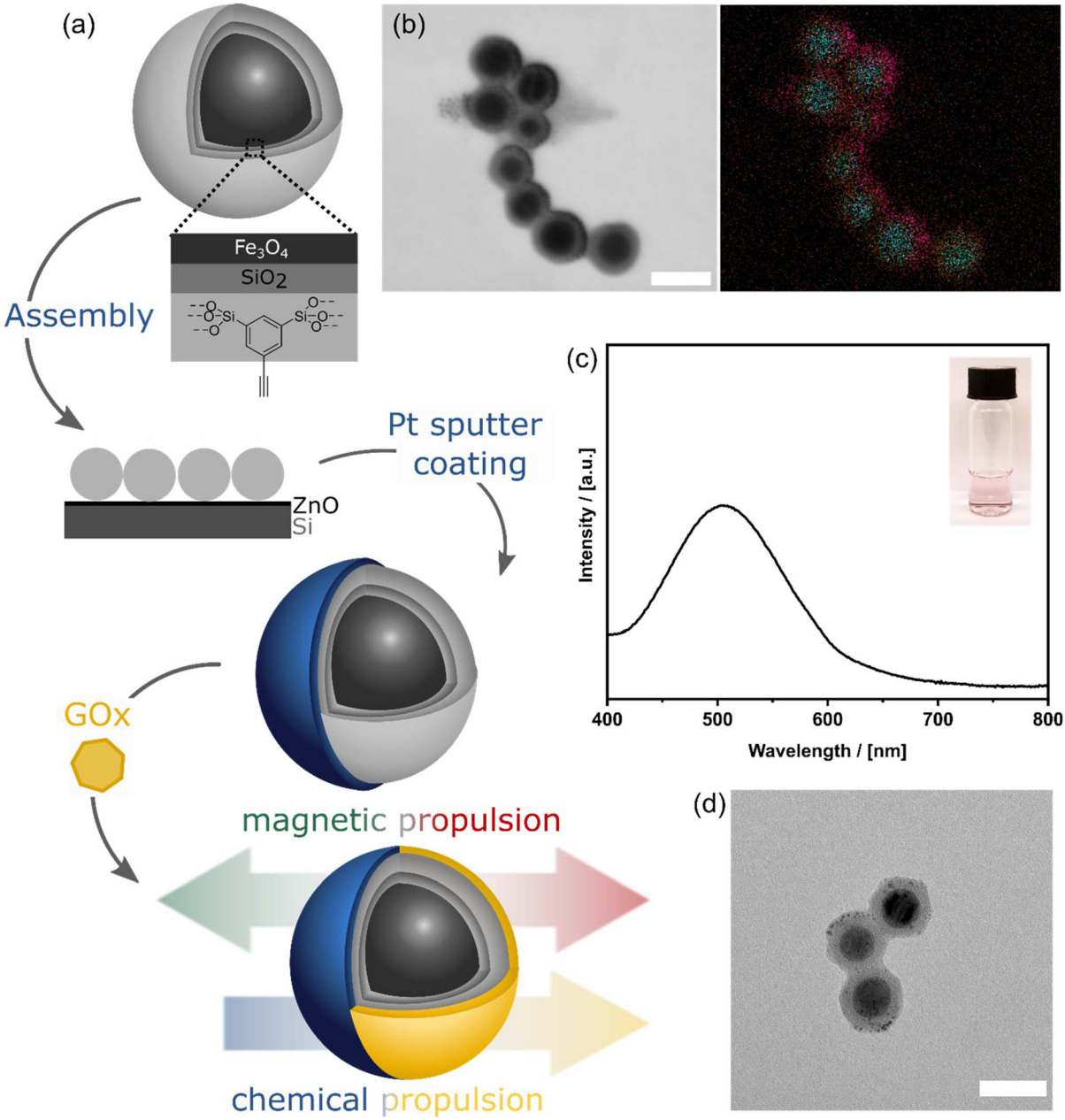

Fig. 1 (a) Scheme showing the Janus nanomotor architecture and the different steps in the chemical functionalization of the organosilica surface. (b) STEM image and EDX mapping of CS@Pt nanoparticles with Fe in blue, Si in orange, and Pt in pink, scalebar 50 nm. (c) UV/Vis spectrum of the enzymatic assay with CS@Pt|GOx nanoparticles. The inset shows a colored assay of CS@Pt|GOx nanoparticles. (d) TEM image of CS@Pt@GOx, scalebar 50 nm.

platinum (Pt) layer on the upper particle hemisphere (see ESI Fig. S2†). The resulting particles (CS@Pt) can be released from the substrate by dissolving the ZnO layer on the wafer under acidic conditions.

The anisotropic positioning of the platinum nanocrystals on CS is confirmed by scanning transmission electron microscope (STEM) imaging by taking advantage of the enhanced imaging contrast of Pt compared to the organosilica phase and also in energy-dispersive X-ray (EDX) mapping of Pt, see Fig. 1b. Because one cannot avoid agglomeration of the particles during the preparation of the samples for electron microscopy, their orientation on the grid is random. Therefore, one sees the Pt-containing hemisphere from different perspectives. When we disperse the particles, stable colloidal solutions are obtained, and according to DLS there is no dominant aggregation process. Further characterization data of CS@Pt and experiments addressing the catalytic activity are shown in ESI Fig. S2.† Next, the remaining hemisphere of CS@Pt becomes functionalized with the enzyme GOx. By adapting the method of Wu *et al.* the enzyme gets co-

valently bound to the particle's surface *via* the thiol–yne click reaction of 11-mercaptoundecanoic acid and activation of the carbonic acid groups (see Fig. S3a†).[38] The covalently bound enzyme is catalytically active after attachment, as shown by a color change in the enzymatic assay in Fig. 1c (for further data, see ESI Fig. S3†). Electron microscopy images of the resulting CS@Pt|GOx colloids are shown Fig. 1d.

Magnetic propulsion mode

Nanoparticle tracking analysis (NTA) is used to investigate the mobility of the CS@Pt|GOx colloids under different conditions. As expected, the CS@Pt|GOx exhibit Brownian motion when none of the two engines is activated (see Fig. 2b and ESI Videos S1†). The physically induced particle movement is initiated by applying an external magnetic field from a permanent magnet (580 mT). The magnetic field is inhomogeneous under such conditions and,[39] despite the superparamagnetic nature of the nanoparticles, allows them to be accelerated. The strength of the magnetic field depends on distance ($\propto r^{-3}$), and given the permeability of water (0.999 μ/μ^0) it decays to ≈90 nT at 0.3 cm, which is the maximum distance used in our experiments. The magnet was placed at different positions to change the direction of the magnetic field B (Fig. 2a) and, accordingly, the direction of acceleration (see ESI Videos S2 and S3†). Fig. 2b shows the trace of one representative particle. It can be seen that the colloid responds to the external field leading by an enhanced and directed motion. Quantifying the particle's mobility was achieved by determining the mean square displacement function (MSD) as a function of time from NTA videos, see ESI Fig. S4a.† The MSD increases linearly after switching on the magnetic field from $MSD_{B=0}$ = 28.5 μm^2 to MSD_{magn} = 53.4 μm^2 (MSD value after 3 s). The effective diffusion coefficient (D_{eff}) can be calculated from the slope of the MSD and increases from 1.6 without propulsion to 2.8 μm^2 s^{-1} under magnetic propulsion, see Fig. 2c.

Because we know the size of the particles (see Fig. 1), one can estimate the average speed of the particles (v). The increase of $v_{B=0}$ = 96.1 ± 6.5 bodylength per s (≈4.5 × 10^3 nm s^{-1}) to v_{mag} = 499.3 ± 34.1 bodylength per s (≈2.4 × 10^4 nm s^{-1}) is indicative of a strong acceleration even by the weak magnetic field we have used. Altering the field strength is interesting too, but this approach was not included in the work we present herein. While we can see that the overall mobility has increased because of the magnetic field, further evaluation of the data is necessary to conclude information about the directionality of the movement. The ratio of motion (RoM) is defined by the ratio of the diameter of a circle fitting to the motion trajectories (see ESI Fig. 4b†). The higher the RoM value is, the more directed the motion of the nanomotors. The evaluation for CS@Pt|GOx indicates a RoM factor of ~5 (Fig. 2c) meaning the particles move significantly stronger into the direction of the field compared to the field-free state. As expected, the CS nanoparticles – without anisotropic surface functionalization behave similar under magnetic propulsion conditions, as can be seen in Fig. S4c and d.†

Chemical propulsion mode

The two-step mechanism of the chemical engine operating with glucose was already mentioned (Fig. 3a). The gaseous oxygen generated at one of the Janus particle's surfaces exerts a bubble propulsion effect (Fig. 3a). The MSD analysis of CS@Pt|GOx nanomotors at different fuel concentrations (see ESI Fig. S5a†) shows that using 50 mM glucose (homogeneously distributed in solution) results in the highest mobility.

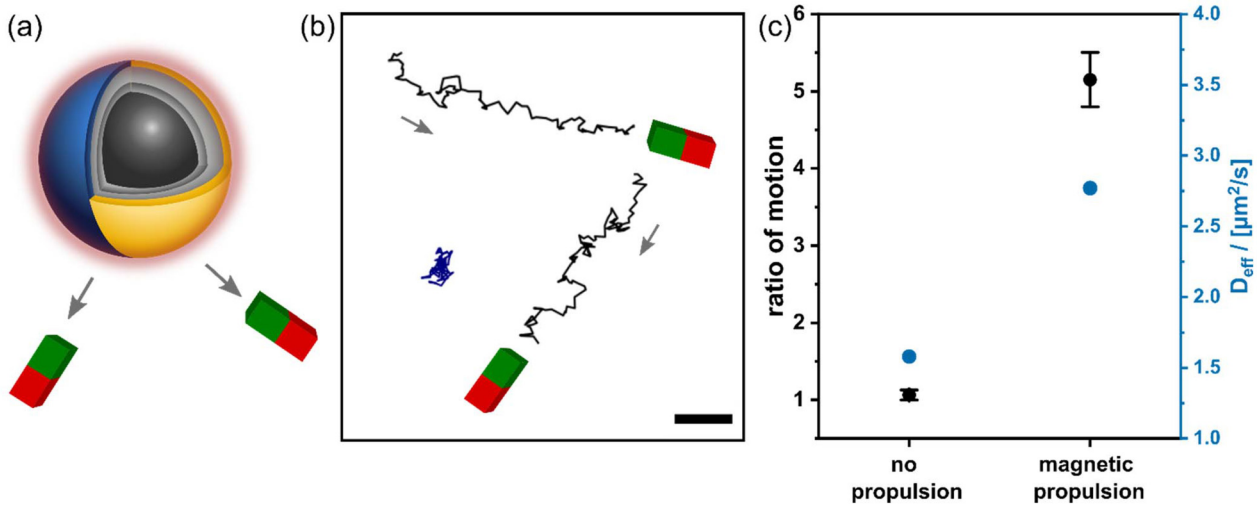

Fig. 2 (a) Schematic depiction of magnetic propulsion mode of CS@Pt|GOx nanomotors; red layer around the nanoparticle indicates the addressed magnetic response by the magnetic field. (b) Trajectories (3 s) of CS@Pt|GOx nanomotors in absence of a magnetic field as a reference (blue) and under magnetic propulsion and different oriented magnetic directions (black). The grey arrow indicates the direction of the CS@Pt|GOx direction; scalebar 20 μm. (c) D_{eff} calculated by MSD and RoM of CS@Pt|GOx nanomotors in the magnetic propulsion mode. RoM: mean value of eight trajectories, error bars refer to standard deviation of RoM.

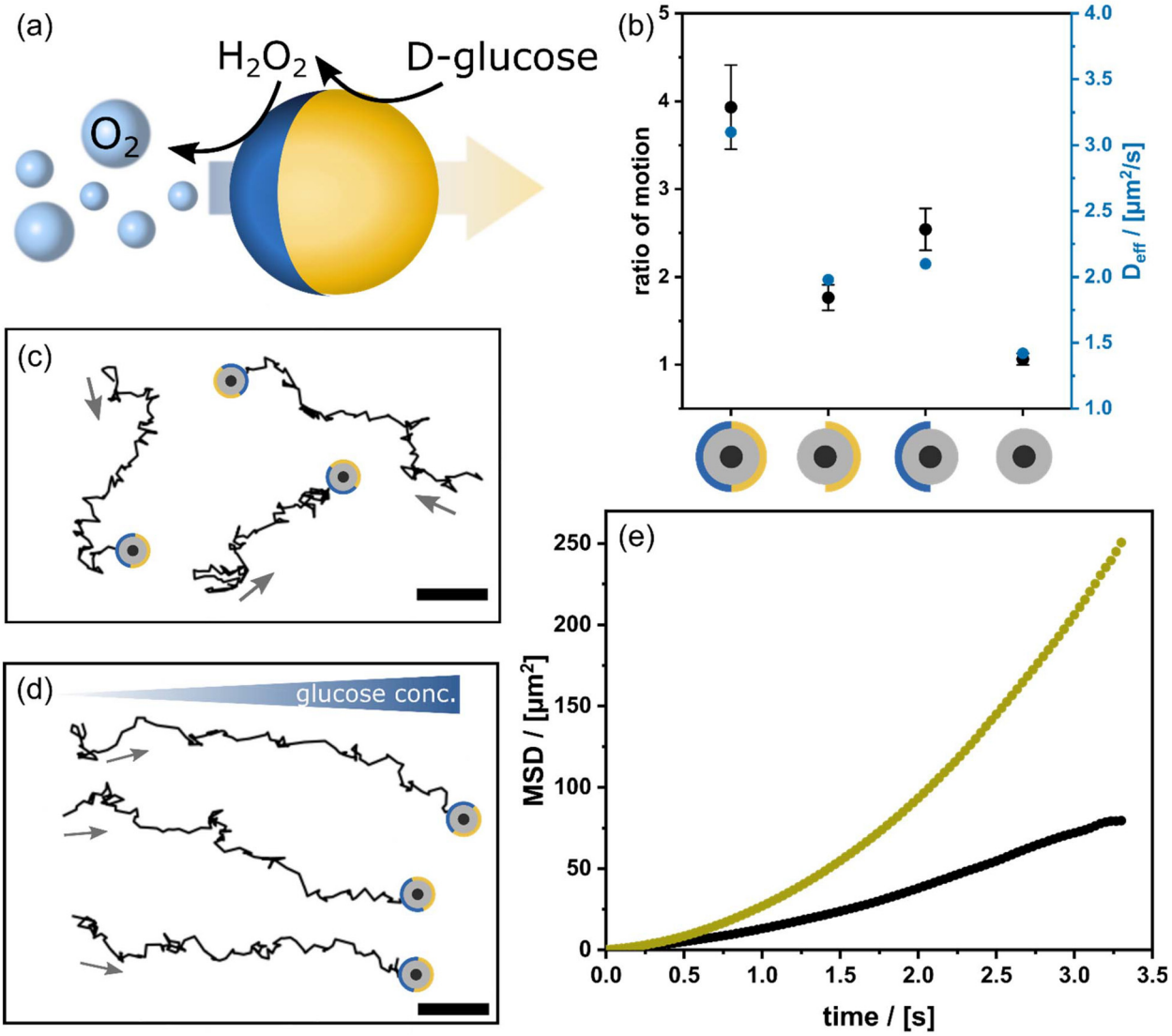

Fig. 3 (a) Schematic depiction of chemical propulsion mode of CS@Pt|GOx nanomotors. (b) D_{eff} calculated by MSD and RoM of CS@Pt|GOx (with 50 mM glucose), CS@GOx (with 50 mM glucose), CS@Pt (with 0.1 wt% H_2O_2) and CS (with 50 mM glucose) nanoparticles under chemical propulsion mode. RoM: mean value of eight trajectories, error bars refer to standard deviation of RoM. (c) Trajectories (3 s) of CS@Pt|GOx nanomotors under chemical propulsion (50 mM glucose) with homogenously distributed fuel, grey arrow indicates moving direction of nanomotors, scalebar 20 µm. (d) Trajectories (3 s) of CS@Pt|GOx nanomotors under chemical propulsion with gradient fuel, grey arrow indicates moving direction of nanomotors, scalebar 20 µm. (e) MSD of CS@Pt|GOx nanomotors with homogenously distributed fuel (black) and a fuel gradient (green).

At even higher glucose concentrations, the viscosity of the solution is increased, which hinders the nanomotors' motion. This result is also reflected by the maximum D_{eff} = 3.1 µm^2 s^{-1}, a RoM = 3.9, and a speed of 381.2 ± 46.3 bodylenght per s at 50 mM glucose, see Fig. 3b and ESI Fig. S5b.†

To assess the effectiveness of CS@Pt|GOx the latter results are compared to colloids missing the corresponding part in the Janus structure: CS@Pt, CS@GOx and CS. CS@Pt is powered by the direct addition of H_2O_2; thus, bubble propulsion occurs too. Because CS@GOx is treated with glucose and there is no gas formation, the propulsion shows a low impact. The control CS nanoparticles are studied with glucose as well as H_2O_2 as fuel and demonstrate that a modification is needed to consume the fuel, as can be seen in Fig. 3b and S5.† Acceleration is maximized in the CS@Pt|GOx case (see ESI Fig. S5†), which proves the synergy of the chemical functionalities. The direction of the movement is random Fig. 3c which is not surprising because the orientation of the colloids is statistical (see also ESI Video S4†). The situation changes when glucose concentration is not homogenous anymore, but a concentration gradient is applied (Fig. 3d). All colloids move in the same direction, towards higher glucose concentration, respectively (see also ESI Video S5†). In agreement the RoM increases by a factor of 6.8. The parabolic increase of the MSD (t) curve shown in Fig. 3e indicated an active transport under gradient conditions.[40] D_{eff} changes from 3.1 to 5.4 µm^2 per s

for the gradient glucose field (see ESI Fig. S5†). The average speed ($v_{chem,grad}$ = 660.5 ± 32.0 bodylength per s) exceeds that of the magnetic propulsion mechanism, which also led to an anisotropic movement (Fig. 2).

At first glance, these results seem to be counterintuitive. Due to the small size of the particles, rotational diffusion is expected to be the main contribution to the motion of the nanomotors. However, the presented increase in MSD and ROM clearly implies, that a significant part of the motion has to be translational diffusion, which is in agreement with studies of Lee *et al.* at a similar size regime.[13]

Dual propulsion mode

The two types of engines are independent of each other capable of producing a directed movement of the CS@Pt|GOx colloids. We can proceed by investigating the system when the dual triggers are active at the same time. When the magnetic and the chemical field point into the same direction, a_{mag} and

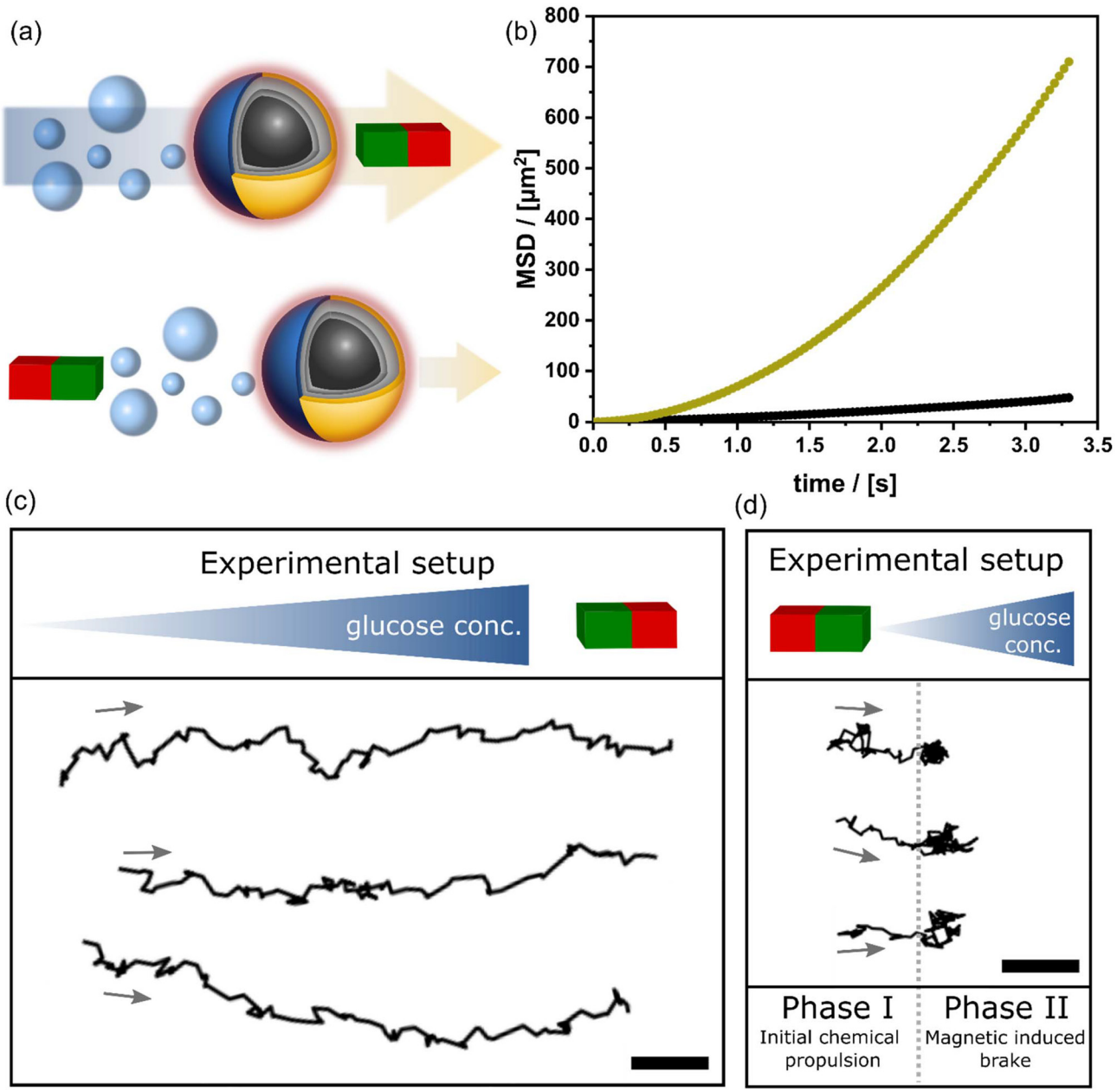

Fig. 4 (a) Schematic depiction of dual propulsion mode of CS@Pt|GOx nanomotors with boost and brake mode; red layer around the nanoparticle indicates the addressed magnetic response by the magnetic field. (b) MSD of CS@Pt|GOx nanomotors boost mode (green) and brake mode (black). (c) Trajectories (3 s) of CS@Pt|GOx nanomotors in boost mode with same orientation of glucose gradient and magnetic field; scalebar 20 µm. (d) Trajectories (3 s) of CS@Pt|GOx nanomotors in brake mode with opposite orientation of glucose gradient and magnetic field. Applying the magnetic field induces the brake mode; scalebar 20 µm.

a_{chem} should add up in an ideal case (Fig. 4). The analysis of the trajectories reveals what we call a "boost mode". Indeed, the diffusion coefficient ($D_{eff,mag+chem}$ = 14.5 μm^2 s^{-1}) is five-fold, and $v_{mag+chem}$ ≈4.62 × 10^4 nm s^{-1} is almost doubled compared to v_{mag} (≈2.4 × 10^4 nm s^{-1}). The high RoM value (=10.2) proves that the movement direction has become even more anisotropic (see Fig. 4c and ESI Video S6†). It is clear that the direction of the chemical gradient cannot be changed during the experiment. In contrast, one can instantly change the direction and strength of the magnetic field. This possibility unravels the most fascinating feature of our system. If a_{mag} is only slightly larger than a_{chem}, one can effectively slow down the colloids or even make them halt. Therefore, we have called this situation the "brake mode". The result of our experiments is shown in Fig. 4d and can be explained by distinguishing between two phases. In phase I, the particles behave as known in the chemical propulsion with glucose gradient. They move collectively into the direction of higher glucose concentration. Switching on the magnetic propulsion by placing the magnet in opposite direction of the glucose gradient initializes phase II. The CS@Pt|GOx nanomotors stop abruptly, as can be seen by the trajectories in Fig. 4d (right side and ESI Video S7†). Although, the results show the values including phase I and II, all mobility values are now close to the ones of colloids without any active forces acting on them (RoM = 2.5, MSD = 47.7 μm^2 and D_{eff} = 2.2 μm^2 s^{-1}). The strong decrease in the MSD illustrates the high impact of the brake mode after entering phase II. This work focuses on a proof of concept of dual nanomotors with flexible operation of the magnetic component which can be seen in the evaluation of RoM, MSD and D_{eff}. Further deep diving into the mechanisms of the switch between boost and brake mode could clarify the chemotactic drift and thereby reveal, whether the magnetic drift and chemical propulsion act independently or if an interplay of the two motion mechanisms takes place. Literature offers promising examples of such analysis *via* studies on dynamic models and simulations.[41,42]

Conclusions

We have presented novel colloids in which the angle between the propulsion between a chemical motor and a physical impetus can the adjusted independently (Scheme 1). Compared to the existing literature on micrometer large colloids, we have prepared nanoscaled particles with Janus architecture and dual propulsion mechanism. It could be shown that one is able to control the movement of those particles with high precision despite of the high relevance of rotational degrees of freedom for such small particles.

The full potential of the system unravels if both associated accelerations are anisotropic. The direction and value of the magnetic acceleration can be changed rapidly, which has several implications. (1) One can bring colloids to a particular position and then halt them at this place. Such a feature may be used in the future for a quantitative study of chemotaxis. Currently, we do not know exactly if the dual acceleration is a simple superposition of magnetic drift and chemical self-propulsion or whether there is some interplay between the two motion mechanisms. Once this is clarified, for a defined magnetic field strength and magnetic properties of the particles, one can envision concluding the quantitative correlations about the chemotactic drift based on the trajectory data of the particles. Unlike spherical nanoparticles reported here,[34] those with a rod-like magnetite core[35] could experience a torque when a magnetic field is applied. Thus, such elongated colloids could be even more promising in the future for investigating chemotaxis. (2) A permanently accelerated colloid cannot reach a steady state equilibrium. One can imagine that an oscillating magnetic field would push CS@Pt|GOx colloids permanently from a "boost mode" to the "break mode" and back. (3) A transition from Brownian to directed motion is connected to a characteristic time scale τ. Simple considerations only regard the rotational diffusion constant D_R ($\tau = 1/D_R$). More refined models have been developed recently to describe the time scale of actively moving Brownian particles.[43] In the future, it will be interesting to probe the rotational behavior of the particles and apply the described models. (4) We have investigated the nanoparticle dispersion only at low concentrations. However, it will be interesting to increase the concentration and see how the non-equilibrium and dissipative conditions act on the system.

All of the mentioned research tasks necessitate a much more controlled magnetic field than in our current proof-of-concept study. We have used a permanent magnet, and the magnetic field strength acting on the particles can only be estimated. Higher fields and more defined conditions are possible using an electromagnet or a superconducting magnet. According experiments are planned in the future.

Author contributions

CL: methodology, synthesis, data curation, formal analysis, investigation, writing-original draft. NK: synthesis, data collection. YK: supervision, verification, project administration. SP: conceptualization, supervision, funding acquisition, project administration, writing-original draft.

Data availability

The data supporting this article have been included as part of the ESI.†

Conflicts of interest

There are no conflicts to declare.

Acknowledgements

Part of this work was funded by the German Research Foundation (Deutsche Forschungsgemeinschaft, DFG) under Germany's excellence strategy within the cluster of excellence PhoenixD (EXC 2122). Analytical measurements were performed in the central analytical facility cfMATCH. We gratefully acknowledge instrumental support (NTA) from the institute of physical chemistry at Leibniz University Hannover. We thank K. Rautmann for writing the script in python for the analysis of the nanomotor tracks.

References

1 D. Needleman and Z. Dogic, *Nat. Rev. Mater.*, 2017, **2**, 17048.
2 G. Gompper, R. G. Winkler and S. Kale, *J. Phys.: Condens. Matter*, 2020, **32**, 193001.
3 K. Villa and M. Pumera, *Chem. Soc. Rev.*, 2019, **48**, 4966–4978.
4 L. K. E. A. Abdelmohsen, M. Nijemeisland, G. M. Pawar, G.-J. A. Janssen, R. J. M. Nolte, J. C. M. van Hest and D. A. Wilson, *ACS Nano*, 2016, **10**, 2652–2660.
5 M. Mathesh, J. Sun and D. A. Wilson, *J. Mater. Chem. B*, 2020, **8**, 7319–7334.
6 W. Gao, X. Feng, A. Pei, Y. Gu, J. Li and J. Wang, *Nanoscale*, 2013, **5**, 4696–4700.
7 A. Zoettl and H. Stark, *J. Phys.: Condens.Matter*, 2016, **28**, 253001.
8 T. Baeuerle, R. C. Loeffler and C. Bechinger, *Nat. Commun.*, 2020, **11**, 2547.
9 A. Ghosh, W. Xu, N. Gupta and D. H. Gracias, *Nano Today*, 2020, **31**, 100836.
10 M. Guix, S. M. Weiz, O. G. Schmidt and M. Medina-Sánchez, *Part. Part. Syst. Charact.*, 2018, **35**, 1700382.
11 R. Dong, Y. Cai, Y. Yang, W. Gao and B. Ren, *Acc. Chem. Res.*, 2018, **51**, 1940–1947.
12 Y. Ji, X. Lin, H. Zhang, Y. Wu, J. Li and Q. He, *Angew. Chem., Int. Ed.*, 2019, **58**, 4184–4188.
13 T.-C. Lee, M. Alarcón-Correa, C. Miksch, K. Hahn, J. G. Gibbs and P. Fischer, *Nano Lett.*, 2014, **14**, 2407–2412.
14 S. Sánchez, L. Soler and J. Katuri, *Angew. Chem., Int. Ed.*, 2015, **54**, 1414–1444.
15 X. Ma, A. Jannasch, U.-R. Albrecht, K. Hahn, A. Miguel-López, E. Schäffer and S. Sánchez, *Nano Lett.*, 2015, **15**, 7043–7050.
16 T. Patiño, N. Feiner-Gracia, X. Arqué, A. Miguel-López, A. Jannasch, T. Stumpp, E. Schäffer, L. Albertazzi and S. Sánchez, *J. Am. Chem. Soc.*, 2018, **140**, 7896–7903.
17 X. Ma, K. Hahn and S. Sanchez, *J. Am. Chem. Soc.*, 2015, **137**, 4976–4979.
18 H. Lv, Y. Xing, X. Du, T. Xu and X. Zhang, *Soft Matter*, 2020, **16**, 4961–4968.
19 L. Baraban, D. Makarov, R. Streubel, I. Mönch, D. Grimm, S. Sanchez and O. G. Schmidt, *ACS Nano*, 2012, **6**, 3383–3389.
20 L. Baraban, D. Makarov, O. G. Schmidt, G. Cuniberti, P. Leiderer and A. Erbe, *Nanoscale*, 2013, **5**, 1332–1336.
21 S. Das, E. B. Steager, M. A. Hsieh, K. J. Stebe and V. Kumar, *J. Microbio Robot.*, 2018, **14**, 25–34.
22 P. S. Schattling, M. A. Ramos-Docampo, V. Salgueiriño and B. Städler, *ACS Nano*, 2017, **11**, 3973–3983.
23 C. M. Oral and M. Pumera, *Nanoscale*, 2023, **15**, 8491–8507.
24 B. Wang, S. Handschuh-Wang, J. Shen, X. Zhou, Z. Guo, W. Liu, M. Pumera and L. Zhang, *Adv. Mater.*, 2023, **35**, 2205732.
25 F. Ji, Y. Wu, M. Pumera and L. Zhang, *Adv. Mater.*, 2023, **35**, 2203959.
26 C. Chen, F. Soto, E. Karshalev, J. Li and J. Wang, *Adv. Funct. Mater.*, 2019, **29**, 1806290.
27 C. Chen, S. Tang, H. Teymourian, E. Karshalev, F. Zhang, J. Li, F. Mou, Y. Liang, J. Guan and J. Wang, *Angew. Chem., Int. Ed.*, 2018, **57**, 8110–8114.
28 J. Shao, S. Cao, H. Che, M. T. De Martino, H. Wu, L. K. E. A. Abdelmohsen and J. C. M. van Hest, *J. Am. Chem. Soc.*, 2022, **144**, 11246–11252.
29 M. Liu, L. Chen, Z. Zhao, M. Liu, T. Zhao, Y. Ma, Q. Zhou, Y. S. Ibrahim, A. A. Elzatahry, X. Li and D. Zhao, *J. Am. Chem. Soc.*, 2022, **144**, 3892–3901.
30 Z. Ye, Y. Wang, S. Liu, D. Xu, W. Wang and X. Ma, *J. Am. Chem. Soc.*, 2021, **143**, 15063–15072.
31 J. Li, T. Li, T. Xu, M. Kiristi, W. Liu, Z. Wu and J. Wang, *Nano Lett.*, 2015, **15**, 4814–4821.
32 W. Gao, K. M. Manesh, J. Hua, S. Sattayasamitsathit and J. Wang, *Small*, 2011, **7**, 2047–2051.
33 A. A. Solovev, S. Sanchez, M. Pumera, Y. F. Mei and O. G. Schmidt, *Adv. Funct. Mater.*, 2010, **20**, 2430–2435.
34 C. Lanz, M. Schlötter, N. Klinkenberg, P. Besirske and S. Polarz, *Angew. Chem., Int. Ed.*, 2020, **59**, 8902–8906.
35 C. Lanz, Y. Krysiak, X. Liu, M. Hohgardt, P. J. Walla and S. Polarz, *Small*, 2023, 2304380.
36 H. L. Ding, Y. X. Zhang and S. Wang, *Chem. Mater.*, 2012, **24**, 4572–4580.
37 R. Hoogenboom, *Angew. Chem., Int. Ed.*, 2010, **49**, 3415–3417.
38 H. Wu, Y. Liang, J. Shi, X. Wang, D. Yang and Z. Jiang, *Mater. Sci. Eng., C*, 2013, 8.
39 K. Zahn, R. Lenke and G. Maret, *Phys. Rev. Lett.*, 1999, **82**, 2721–2724.
40 V. Briane, M. Vimond and C. Kervrann, *Briefings Bioinf.*, 2020, **21**, 1136–1150.
41 T. Li, Z. Liu, J. Hu, L. Chen, T. Chen, Q. Tang, B. Yu, B. Zhao, C. Mao and M. Wan, *Adv. Mater.*, 2022, **34**, 2206654.
42 M. N. Popescu, W. E. Uspal, C. Bechinger and P. Fischer, *Nano Lett.*, 2018, **18**, 5345–5349.
43 L. Fang, L. L. Li, J. S. Guo, Y. W. Liu and X. R. Huang, *Phys. Lett. A*, 2022, **427**, 127934.